ENGINEERING PERSPECTIVE

Research Paper

Study of Subsurface Damage of Tungsten Alloy in Rotary Ultrasonic Grinding

Emmanuel Karangwa, Pacifique Turabimana*

Mechanical Engineering Department, IPRC Gishari-Rwanda Polytechnic, Rwamagana, Rwanda

ABSTRACT

Tungsten alloy is generally used in aerospace, military defense services, the nuclear industry, and other essential fields of manufacturing due to its physical and chemical properties. As the demand for tungsten alloy increases, it demands higher requirements for the accuracy, quality, and surface integrity of tungsten alloy products. So, it is of paramount importance to study the manufacturing, processing, and testing of tungsten alloys through the power generating during machining, the surface, and subsurface of finished products. Grinding is an abrasive machining method that can achieve extremely fine surface finishes while retaining high dimensional and shape precision. However, the process causes subsurface damage, which affects the mechanical properties and surface quality of the machined workpiece. In this paper, the grinding simulations in Abaqus software and experiments on CNC machine on both Rotary Ultrasonic Grinding (RUG) and Conventional Grinding (CG) were carried out by Taguchi experimental design method to study the different influences of spindle speed, grinding depth, feed rate, ultrasonic frequency and amplitude on subsurface damage induced in grinding of tungsten alloy. Briefly, simulation and experiment results showed well agreement at the same time present the reduction of subsurface damage depth on ultrasonic grinding compared to conventional grinding. Also, the increase of grinding depth and feed rate and amplitude generates a high Subsurface Damage depth (SSD depth) where the increasing of spindle speed decreases the SSD depth, but ultrasonic frequency present a little effect on it.

Keywords: Tungsten alloy; Rotary ultrasonic grinding; Conventional grinding; Finite element method; Constitutive model; Subsurface damage; and Grinding force.

1. Introduction

Tungsten (W) is dull silver-grey metal with the highest point fusion of almost pure metal. It can be combined with other metals to form tungsten alloys to increase their strength and resistance to wear and corrosion. Because of its physical and chemical properties such as corrosion resistance, radiation safety, high hardness, and good impact efficiency, tungsten alloy is widely used in aerospace, military defense, nuclear industry, and other essential fields. In the past twenty years, due to the high strength, high density, good plasticity, and good machinability of tungsten alloy, tungsten alloy production is increasing in China. In 2003, China's density production of tungsten alloy was about 1139 tons but only six years after the product has been more than 3000 tons per year [1]. The researchers continuously review and improve the effective ways to improve tungsten alloy strength and hardness and toughness. Since conventional machining (CM) can't machine well tungsten alloy precisely due to

rapid tool wear, brittle fracture, and tool adhesion, the ultrasonic machine is applied to machine hard and brittle material [2]. Ultrasonic Machining (USM) is one of many viable machining methods that can process hard and brittle materials regardless of their electrical and mechanical properties, which are usually a constraint for other techniques. In ultrasonic machining, abrasive particles in the form of slurry strike the work surface, causing the material to be extracted. To overcome these several limitations generally, occur in static ultrasonic machining as well as conventional diamond grinding, the RUM (Rotary Ultrasonic Machining) was built. RUM is a hybrid machining process that combines USM and CM to remove material from a workpiece through microchipping and abrasive grinding [3].

As a result, it is critical to conduct a thorough study to examine SSD in grinding processes and to investigate the impact of process parameters on SSD depth. However, the subsurface damage which is introduced to substrates in manufacturing processes may seriously

deteriorate part quality. Aside from production cycle, surface accuracy, and manufacturing expense, it has an effect on operational life, secular stability, coting efficiency, and transmission performance, which has attracted a lot of attention recently [4]. Therefore, it is critical to study the factors that influence the subsurface quality of hard& brittle material in grinding. Detection, measurement, and monitoring of SSD to improve tungsten alloy machining performance and the surface is now one of the optical manufacturing industry's problems to solve [5].

The primary aim of this research is to simulate as well as perform experimental grinding processes for finding the effects of ultrasonic excitation on subsurface damage of tungsten alloy (W-Ni-Fe) to get high quality of products, improve machining efficiency, a quality life of machine parts, time-saving for machining and to minimize production costs by comparing the variations between RUG and CG at the same machining parameters.

2. Detection methods

The SSD is easily generated in the machining operation, to date, there are more researches about the techniques to evaluate and remove the SSD depth for improving the efficiency quality, a lifetime of a machined part, to reduce the cost and the time for machining based on the various methods. The destructive methods can provide measurable, accurate, and quantitative data, they cannot be used to estimate the global information of SSD in a sample. Furthermore, the sample must be destroyed, which takes time and is costly. In production methods that are rigid and production in large quantities, the detection cost is sufficient. Non-destructive methods, on other hand, are more applicable and effective. Customized parts will become more common in the future, necessitating this method for estimating the SSD initiated in a part easily. Non-destructive methods are often simpler to incorporate into a line of products and they are needed to be developed to satisfy the rising demand for high-quality manufacturing products.

2.1 Different Detection methods

The most popular method for SSD detection and observation is traditional taper polishing. A sample is cut at an angle β to the machined surface and then the cut surface of the sample is polished to minimize any damage caused by the cutting process. The polished sample is engraved to remove the polished surface's layer, exposing the SSD, which is then examined under microscopy and the SSD depth measured. The SSD depth (H) is calculated as Eq.1 [6].

$$H = L \times sin\beta \qquad (1)$$

The University of Rochester's optical manufacturing center [7] developed a dimpling method to find out SSD. This method polishes a sample part with a steel ball to create a dimple in series to reveal the SSD of the part, similar to the conventional taper polishing method. The depth of the dimple is sufficient to pass through the damage layer matrix. The SSD depth is determined by calculating the characteristic dimensions of a dimple. It is quick to operate and inexpensive. The MRF(Magnetorheological Finishing) polishing has been utilized in SSD measurement since the advent of precision ma-

chining technology [8]. Mulhern et al proposed the Bonded-Interface Technique (BIT) to look at the material deformation of metals in an indentation test [9]. Figure 1 illustrates the BIT schematics, which are subdivided into several steps. The first step was to polish the surfaces that had to be glued together; second, glue was used to bind the polished surfaces; third, the work surface was machined; finally, the bonding glue was removed, and SSD was observed using a microscope on the two polished interfaces.
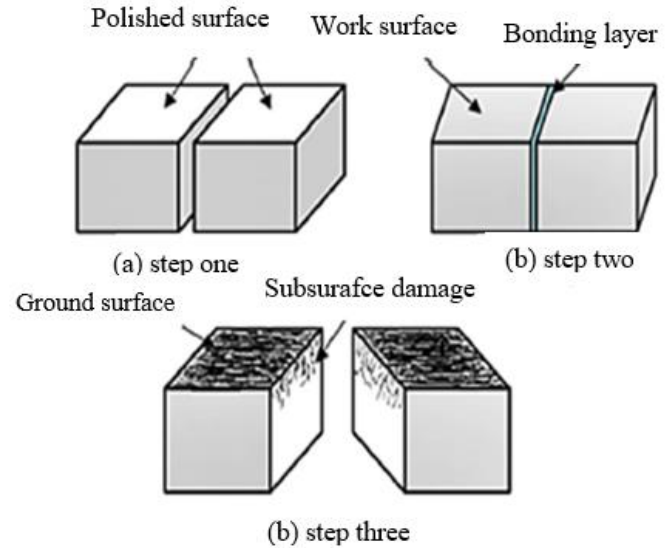

Figure 1. Schematics of bonded interface techniques

Several technologies have been proposed to detect SSD with laser scattering. Temple et al used Total Internal Reflection Microscopy (TIRM) to detect surface and subsurface damage of the transparent samples, and several other researchers applied TIRM to optical materials later [10]. Lambropoulos [11] suggested a relationship between the depth of the damage and the size of abrasive grains. Focused on indentation fracture mechanics, Wang et al [12] hypothesized that SSD formation was caused by brittle workpiece material fracture, and proposed an explicit equation to predict SSD depth as shown in equations 2.

$$\frac{\delta}{SR} = 2.326\alpha_k^{\frac{2}{3}} \left(\frac{E}{H}\right)^{\frac{2-5m}{3}} \frac{(cot\Psi)^{\frac{1}{9}}}{(sin\Psi)^{\frac{1}{2}}} \left(\frac{P}{\frac{k_c^4}{H^3}}\right)^{\frac{1}{6}} \qquad (2)$$

where E, H, and Kc are the elastic modulus, the hardness, and the toughness of the workpiece material respectively, δ is SSD depth, SR is surface roughness, ψ is the semi-angle of the sharp cone of an abrasive grain; P is the force acting on the grain. α_K and m are numerical factors. Force P determines the ratio, yet in practical machining, it varied with process parameters, which renders the model inconvenient to use. Xiao et al [13], enhanced the model in equation 2, by stating the relation between SSD and Ra as nonlinear by eliminating grain force P,

$$\delta = 3.08\alpha_k^{\frac{2}{3}} \frac{1}{(sin\Psi)^{\frac{2}{3}}} \frac{H^{2m}}{E^{2m-\frac{2}{3}}K_C} SR^{\frac{4}{3}} \qquad (3)$$

Feng and Zhang [14] correlated SSD depth with cutting force in the RUFM of a K9 glass. They found that SSD depth was proportional to the exponent of cutting force ($\delta = Y F_C{}^X$). Lakhdari et al [15], discovered that the SSD depth caused RUAG was 35% less than CG.

Figure 2, depicts the crack mechanism of brittle material caused by indentation with a sharp indenter, according to indentation fracture mechanics.
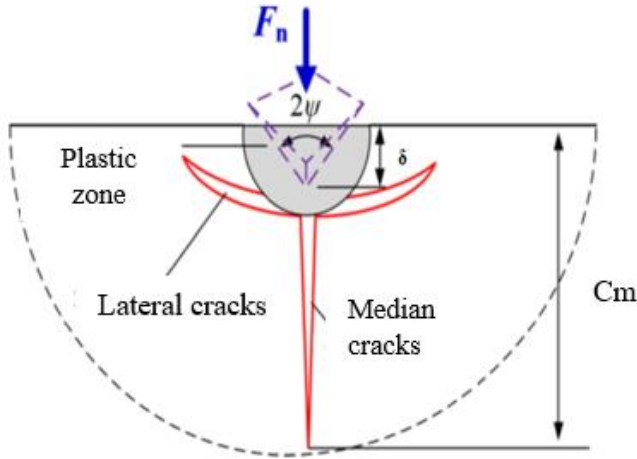

Figure 2. Diagram of crack system caused by a sharp indenter

Where F_n is maximum impact force acting on the workpiece one diamond particle, Ψ is semi angle between two opposite edges of an abrasive particle, δ is the maximum penetration depth of single abrasive particle penetration into the workpiece and Cm is a depth of median crack from the unprocessed surface. The magnitude of Cm determines the SSD characteristic in RUFM of optical glass. Based on indentation fracture mechanics, Lambropoulos et al, developed the calculation formula of Cm as flows:

$$C_m = \alpha_k^{\frac{2}{3}} \left(\frac{E}{H_v}\right)^{(1-q)\frac{2}{3}} (\cot\Psi)^{\frac{4}{9}} \left(\frac{F_n}{K_{1c}}\right)^{\frac{2}{3}} \tag{4}$$

Where E is elastic modulus, H_v is micro-hardness, K_1c is fracture toughness, q is a dimensionless coefficient to correction. They found that the depth of SSD is directly proportional to the exponent of measured cutting force as seen in Equations 5.
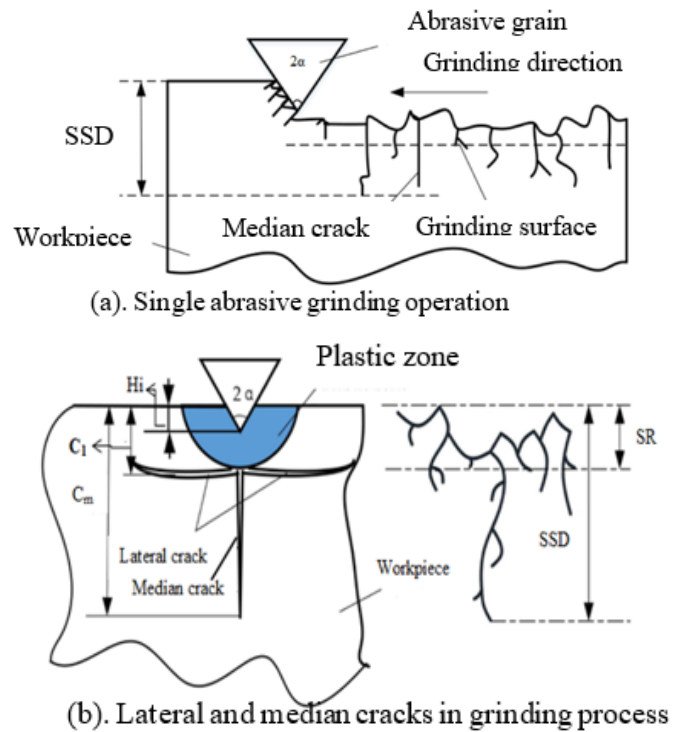
$$d_{SSD} = y F_c{}^x \tag{5}$$

Where d_{SSD} is the predictive SSD depth, γ is the proportionality factor, and x is the index of the power function. this method has shown that under the same processing conditions, the measured cutting force in RUFM is much smaller than in CG and also the estimated cutting force follows the variance trend of SSD depth with an increase in processing parameters [16].

In the study of cracks in ceramic damage, Liu et al used utilized computational simulation to assess the degree of damage [17]. The simulation results have been shown that Ultrasonic Vibration Machining (UVM) can effectively reduce the average cutting force and reduce the cutting temperature at tooltip compared with

Con-ventional Machining (CM) and maximum misses stress show that UVM can effectively reduce the machining stress, the larger amplitude corresponds to smaller max-imum misses' stress. Moreover, the cutting effects are further improved with an increment of vibration ampli-tude under set conditions.

Linlin carried out an FEA method on silicon nitride grinding based on virtual abrasive with a truncated pol-yhedral shape to simulate the subsurface depth. The influence factors of the grinding parameters on subsur-face damage depth were analyzed. The average error between prediction and experiment results was approx-imately 9%, which validated the prediction accuracy and generalization ability of the prediction model. Also, the SSD depth increased with the increment of work-piece speed and grinding depth, while as the speed in-creased, the SSD depth decreased [18].

Yan Gu studied the theoretical analysis on the SSD model for polishing the SiC ceramic, and discovered that the contact grinding of material can be intuitively condensed into a single grit scratch processing [19], as shown in Figure 3 (a), while figure 2-3 (b), illustrates the lateral and median cracks in detail. The SSD is caused by a median crack.

(a). Single abrasive grinding operation

(b). Lateral and median cracks in grinding process
Figure 3. The Model of subsurface damage

The depth of median crack Cm can be calculated by property of materials, the abrasive grain geometry, and depth of penetration as:

$$Cm = 0.206 \frac{(E \times Hs)^{\frac{1}{3}}}{Kc \times \beta} \ (\cot\alpha)^{\frac{4}{9}} \ (\tan\alpha)^{\frac{4}{3}} \ (Hi)^{\frac{4}{3}} \tag{6}$$

Where Cm is the length of median crack from the base of the plastic region; Cl is the depth of lateral crack from the base of the plastic deformation region; Hi is the abrasive particles penetrating distance into the workpiece; α is the apex angle of abrasive grain, Hs is the scratch hardness, Kc is the fracture toughness, and β is the material factor specified by elastic recover. The SSD depth has been

calculated using mathematical relation of abrasive and workpiece as:

$$SSD=\max(C_m) \tag{7}$$

3. Methodology

The Abaqus explicitly software is used as numerical techniques on finite element analysis (FEA) method for investigating grinding simulation processes. The work-piece was modeled under a 2D model with the grinding diamond wheel. The subsurface damage depth for both grinding with and without ultrasonic was obtained from grinding simulations under the Johnson cook model. The trajectory of a single abrasive particle of the dia-mond tool is analyzed and traced using MATLAB software. For verifying the simulation results obtained from Abaqus, the experiments were conducted on a CNC machine under the same grinding parameters used in the simulation. The same diamond grinding tools were utilized in all grinding tests on both RUG and CG only the ultrasonic supply switched off for the CG pro-cess. The subsurface damage was observed by Scan-ning electron microscope-SEM and analyzed by ImageJ software after the cross-sectioning method of ground workpieces through the polishing machining. For achieving the goals of this research, the important methods and processes used are summarized in the flowing flowchart:
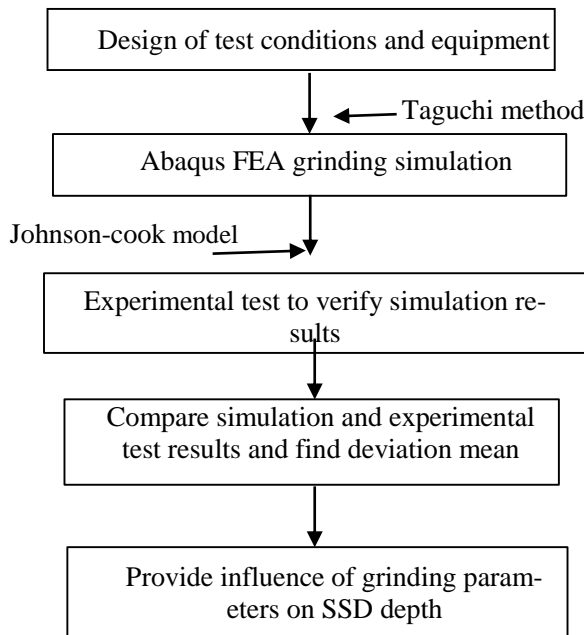

Figure 4. Proposed research methodology

Taguchi design of the experiment method is used in this study. Studying the subsurface damage of tungsten alloy on both RUG and CG, grinding depth, tool spindle speed, feed rate, ultrasonic vibration frequency, and ultrasonic vibration amplitude are selected as grinding parameters in this research. To comparing the RUG and CG results, the study must be done on similar parame-ters, except for RUG, ultrasonic frequency and ampli-tude will be applied. The detail of design plan is shown on table 1 and table 2 below:

Table 1. RUG Experiment conditions

S/N	Parameters	Value
1	Grinding depth (μm)	10, 20, 30
2	Grinding speed (rpm)	4000,5000,6000
3	Feed rate (mm/min)	20, 40, 60
4	Ultrasonic frequency (kHz)	22, 24, 26
5	Ultrasonic amplitude (μm)	1, 2, 3

Table 2. CG Experiment Conditions

S/N	Parameters	Value
1	Grinding depth (μm)	10, 20, 30
2	Grinding speed (rpm)	4000, 5000, 6000
3	Feed rate (mm/min)	20, 40, 60

3.1 FEM simulation modeling

For simulation and modeling machining processes, computational numerical models are becoming increas-ingly relevant [20]. Throughout the features of machin-ing operations, the results of simulation vary significant-ly from experimental results, as many researchers dis-covered, the reason is that numerical models can only reflect physical and mechanical processes in the shear region [21]. The Johnson-Cook model for tungsten alloy is used in grinding simulation for establishing the rela-tion involving the grinding input parameters and grind-ing force generated, as well as residual stress, surface morphology, and SSD. In the practical grinding process, the material removal is produced by the interaction of a large number of random particles distributed on the grinding tool head and workpiece. To make the analysis and computation process easier, a single grit approach is considered where the single grit abrasive grain simula-tion is used to examine the subsurface cracks during grinding tungsten alloy.

The Johnson- cook constitutive equation is the most common for modeling various machining methods, the Johnson- cook formula is as follows:

$$\sigma_s=(A+B\varepsilon^n)[1+C\ln(\tfrac{\dot{\varepsilon}}{\dot{\varepsilon}_0})[1-(\tfrac{T-T_0}{T_m-T_0})^m] \tag{8}$$

Where σs is the stress which causes a material to become plastic, A is the yield strength, B is the strain hardening stress constant, n is the strain hardening power constant, C denotes the strain ratio constant, m denotes the thermal softening power constant, ε is the strain, $\dot{\varepsilon}$ is the strain rate, $\dot{\varepsilon}\_0$ is the value of reference rate of strain, T represents the effective temperature, T0 denotes the room temperature and Tm represents the materials' melting temperature [22].

Also, Johnson-Cook explained the model damage through erosion model by Johnson-Cook failure relying on the impact of plastic strain and presented the damage variable D shown in equation 9.

$$D= \sum \tfrac{\Delta\varepsilon^P}{\varepsilon_f^p} \tag{9}$$

Where $\Delta\varepsilon^P$ represent strain's equivalent plastic in an integration phase, and ε_f^p represents strain's ultimate plastic, which would have the equation 10 as follow:

$$\varepsilon_f^p= \left[D_1+D_2\varepsilon^{D_3\sigma^*}\right][1+D_4\ln(\tfrac{\dot{\varepsilon}_p}{\dot{\varepsilon}_0})][1+D_5 T^*] \tag{10}$$

This grinding simulation 2D model is built and run by using

tungsten alloy properties and Johnson-cook pa-rameters from Bresciani on numerical modeling to re-produce fragmentation of a tungsten heavy alloy [23].

3.2 Construction FEA model

The two-dimensional (2D) model plane is used for building the workpiece and the grinding tool for envisag-ing the formation of lateral and median cracks. Alt-hough the abrasive grains on the surface of the grinding tool have a functional role in grinding. The following are assumptions of the model used:

1. During deformation, the material stayed stable and no chemical changes resulted;

2. The grinding depth was small compared to the size of grit size and the active grinding edge was greater than the depth of grinding;

3. The hardness and strength of the tool were greater compare to those of the workpiece;

4. The period of grinding simulation was severely small and the penalty approach was used in the interac-tion between abrasive and workpiece;

5. The grinding tooltip will slide on the surface of the workpiece at a constant speed and the friction fac-tor of 0.15 was used to identify the tangential and nor-mal friction.

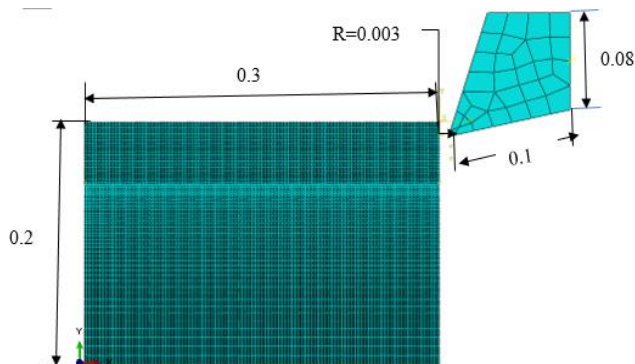6. For dynamic analysis, the approach of mass scaling was used for time calculation.

Figure 5. Abacus FEA numerical simulation model

The experimental tests were done for verifying the simulation results. To observe the SSD of tungsten alloy from experimental tests on both RUG and CG, the workpieces and grinding tools were designed and pro-duced. The specimens are made in tungsten alloy (W-Ni-Fe) while grinding tools are manufactured in dia-mond grit. The cutting wire machining was used to cut into a specimen of 12mm×10mm×3mm as the size of the experiment workpiece. The grinding tool is made in a matrix diamond wheel with 100 particle size and abrasive concentration of 200%, with 10mm× 6mm × 45 mm of the outer, inner diameter, and length of dia-mond grinding wheel respectively.

Both Rotary Ultrasonic Grinding (RUG) and Conven-tional Grinding (CG) tests were conducted on a Machine model called Hanchuan XK714D vertical CNC drilling and milling machine which consists primarily of an ul-trasonic spindle system, a numerical control machining, and coolant system. The ultrasonic spindle system comprises a control panel, power supply, electrical mo-tor, and machining tool in a tool holder.   The data ac-quisition system or numerical control machining system comprises a specimen, machine table, fixture, dyna-mometer, A/D converter, amplifier, and computer while the coolant system comprises with coolant tank, pump, valve, flowrate gauge, pressure regulator, and pressure gauge.

Figure 6.a. Hanchuan XK714D CNC drilling and Mill-ing with all accessories
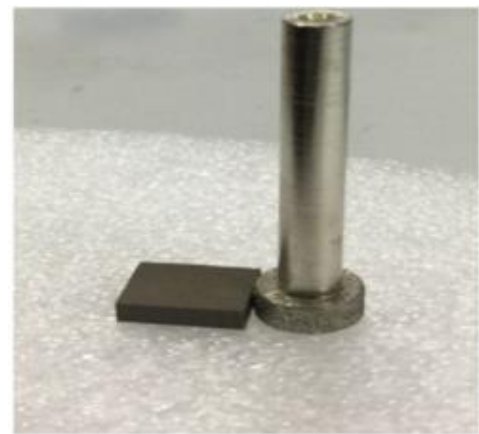

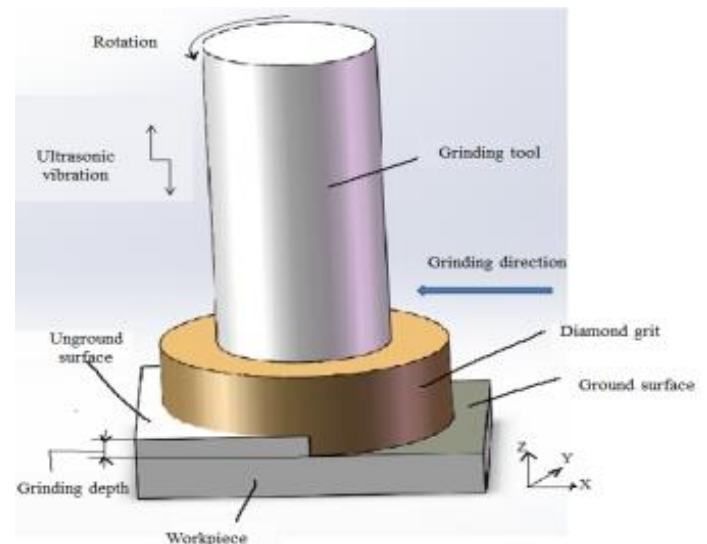Figure 6.b. Grinding tool and workpiece used in the study

Figure 6.c. Designed grinding direction & position

Figure 6.d. Experimental grinding process

3.3 Polishing process and observation of subsurface damage by using SEM

The ground workpieces of 12mm×10mm× 3mm are cut into two equal parts by cutting wire at the surface of 12mm×10mm, and at that time the two-cut polishing backing sheets have the size of 12mm×5mm×3mm of length, width, and thickness respectively. The processed sample surface and the same size surface of the back-ing sheet are bonded together with the glue layer. During bonding, the two samples, the pressure is required to make good bonding joint and tight. The bonding in the pair is shown in Figure 7.
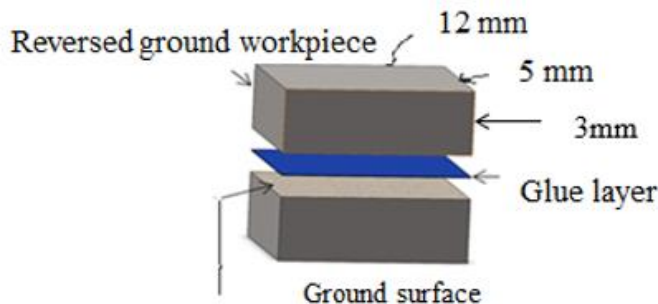

Figure 7. Bonding process and polishing machining

To detect the subsurface damage generated during the grinding process, each ground workpiece was polished on a polishing machine by using 320Cw, 800Cw, 1500Cw, and 2000Cw abrasive polishing paper by us-ing the cross-section polishing method. The grinding time is long enough to ensure the removal of the dam-age caused by the wire cutting process. After polishing the glue layer is

dissolved and the sample is cleaned. The samples were preserved and then observed by SEM and the ImageJ software is used to measure the depth of crack recorded. The Subsurface damage evaluation index was based on maximum damage layer depth which was taken as SSD depth, these damage evalua-tion indexes were recorded during SEM. Then the sub-surface damage obtained on grinding with ultrasonic and conventional grinding were compared.

4. Results and discussion

The existence of subsurface damage seriously affects the performance and life of the workpiece products. In this section, through the orthogonal array tests, the in-fluence of grinding parameters on the depth of subsur-face damage is systematically studied. Based on the subsurface damage results obtained, the subsurface damage characteristics are summarized and analyzed, which can provide a basis for effectively reducing the subsurface damage. Both simulation and experimental SSD depth results are obtained by taking the maximum depth of subsurface damage which are summarized in table 3. The analysis was done based on Orthogonal Experiment Assistant (OEA) software for the Taguchi experiment method on designed simulation grinding parameters.
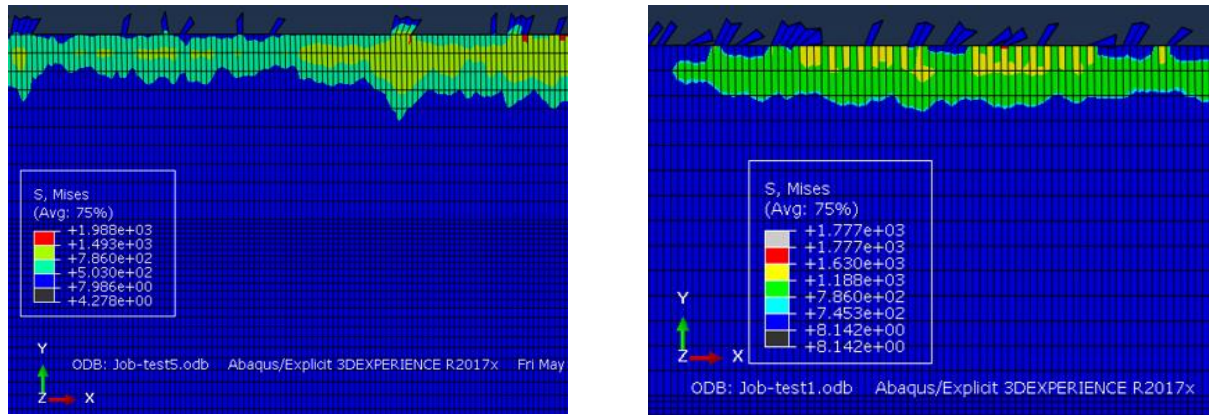
4.1 Simulation SSD depth results

The overall tensile stress is the most key factor monitor-ing the materials' brittle failure as per fracture mechan-ics theory [24]. A brittle fracture happens when a point's maximum tensile stress exceeds the limit stress of a single stress state. Its key aim is to extract material by fracturing and friction, then here in the case of tungsten alloy, the damage appears on the workpiece where if the tensile strength exceeds 786 MPa as bending strength material [18]. As a result, the stress on the grinding surface of the workpiece needs to be assessed. To identify various areas of stress, the counter colors & lines are processed. Once the von mises stress of the built model is over 786 MPa. The magnitude of SSD depth is the maximum SSD depth measured on the ground workpiece by locating the corresponding region in the contour color using the node distance method [25].

The SSD depth simulation results obtained on both RUG and CG are presented in Figure 8. Figure 8 shows some screenshot photos taken to indicates the surface and SSD depth in simulation at different parameters

4.2 Experimental SSD depth results

To verify FEA simulation results, the grinding experiments on both RUG and CG have been conducted three times to confirm the simula-tion results. The experimental SSD depth re-sults obtained by taking the maximum depth of subsurface damage among of five points measured for each ground and polished work-piece on a scanning electron microscopy for three repeated tests are summarized in table 3.

a. RUG at Gd=10μm, Vs=4000rpm, Vw=20mm/min, f=22 kHz, a= 1μm, SSD depth=17.65μm b. CG at Gd=10μm, Vs=4000rpm, Vw=20mm/min, SSD depth=21.50μm

Figure 8. Surface morphology of SSD depth on both RUG and CG

Table3 (a): RUG Orthogonal test simulation and SSD experimental depth results

Test	Gd (μm)	Vs (rpm)	Vw (rpm)	f (rpm)	a (μm)	SIM.SSD depth (μm)	EXP. SSD depth (μm) T1	T2			Deviation (%)
							T3	Average			
1	10	4000	20	22	1	17.65	17.20	18.80	13.5	16.50	6.52
2	10	5000	40	24	2	16.45	16.80	20.10	16.2	17.70	-7.60
3	10	6000	60	26	3	19.40	20.50	16.35	18.95	18.60	4.12
4	20	4000	20	24	2	20.12	19.20	17.45	17.95	18.20	9.54
5	20	5000	40	26	3	18.87	24.10	25.70	21.30	23.70	-25.60
6	20	6000	60	22	1	19.65	16.40	20.18	18.93	18.50	5.85
7	30	4000	40	22	3	23.37	30.18	29.50	27.32	29.00	-24.09
8	30	5000	60	24	1	26.26	23.43	26.40	22.77	24.20	7.84
9	30	6000	20	26	2	16.85	15.78	18.26	16.06	16.70	0.89
10	10	4000	60	26	2	23.75	23.90	24.48	21.52	23.20	2.32
11	10	5000	20	22	3	14.05	15.45	13.65	12.90	14.00	0.36
12	10	6000	40	24	1	14.49	14.00	15.85	14.25	14.70	-1.45
13	20	4000	40	26	1	23.36	22.15	20.40	17.45	20.00	14.38
14	20	5000	60	22	2	22.65	24.70	22.50	20.30	22.50	0.66
15	20	6000	20	24	3	16.05	15.60	13.80	15.18	14.86	7.41
16	30	4000	60	24	3	30.73	30.68	30.50	27.92	29.70	3.35
17	30	5000	20	26	1	20.80	17.50	19.40	19.20	18.70	10.10
18	30	6000	40	22	2	21.76	23.00	20.79	20.71	21.50	1.19
								Average deviation			0.88

Table3 (b). CG orthogonal experiment SSD depth results

| Test	Gd (μm)	Vs (rpm)	Vw (rpm)	SIM.SSD depth (μm)	EXP. SSD depth (μm) T1	T2		T3	Deviation (%)
					Average				
1	10	4000	20	21.45	25.70	26.15	22.40	24.75	13.33
2	10	5000	40	22.40	26.20	24.50	24.60	25.10	10.76
3	10	6000	60	26.65	27.30	28.45	23.60	26.45	-0.76
4	20	4000	40	31.00	40.15	35.46	39.29	38.30	19.06
5	20	5000	60	34.35	39.28	36.78	35.09	37.05	7.29
6	20	6000	20	21.35	20.19	23.45	22.81	22.15	3.61
7	30	4000	60	40.15	45.69	46.38	41.28	44.45	9.67
8	30	5000	20	26.25	30.90	28.10	29.85	29.95	12.35
9	30	6000	40	28.10	34.15	27.45	31.10	30.90	9.06
					Average deviation				9.38

4.3 Trend analysis and influence effects of grinding parameters on SSD depth
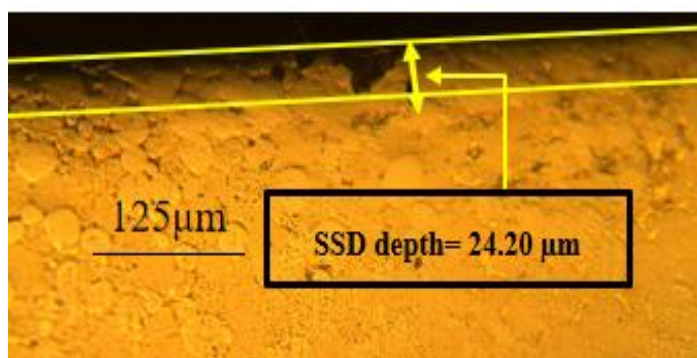
a. Graphical trend on each parameter

The order of influencing of every parameter on RUG SSD depth is feed rate, grinding depth, spindle speed, amplitude, frequency, while for CG SSD depth, it is feed rate, grinding depth, spindle speed respectively for both simulation and experiment as shown on the figure 9. The analysis of the influence of different parame-ters for each level on SSD depth brings the optimized combination of processing parameters.

It can be observed that the SSD depth increas-es with increasing grinding depth, feed rate, and ultrasonic amplitude while the SSD de-creases with increasing grinding spindle speed; the ultrasonic vibration frequency has a little effect on SSD depth which is similar to the numerical simulation result obtained.

According to the range of each parameter and the trend graph, the optimal combination of the SSD depth on RUG is Vw1Gd1Vs3a1f2 and Vw1Gd1Vs3 on RUG and CG respectively. Ac-cording to both numerical simulation and ex-perimental orthogonal test method results, to reduce the subsurface damage depth during selecting machining grinding parameters, the Vw1Gd1Vs3a1f2 optimized combination is sug-gested, where the grinding depth is 10 μm, spindle speed is 6000 rpm, feed rate 20mm/min, the ultrasonic frequency of 24 kHz, and ultrasonic amplitude of 1μm.
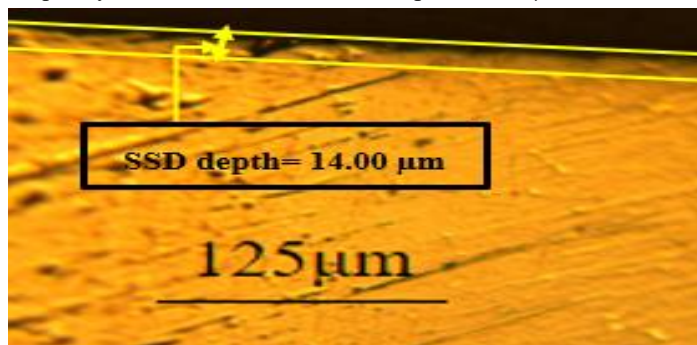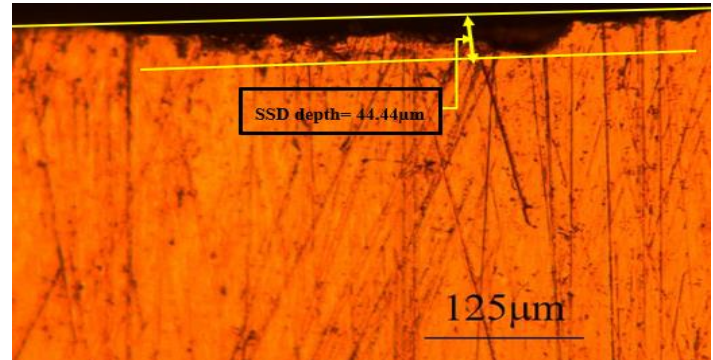

a. RUG at Gd=10μm, Vs=5000rpm, Vw=20mm/min, f=22 kHz, a=1μm

b. RUG at Gd=30μm, Vs=5000rpm, Vw=60mm/min, f=24 kHz, a=1μm
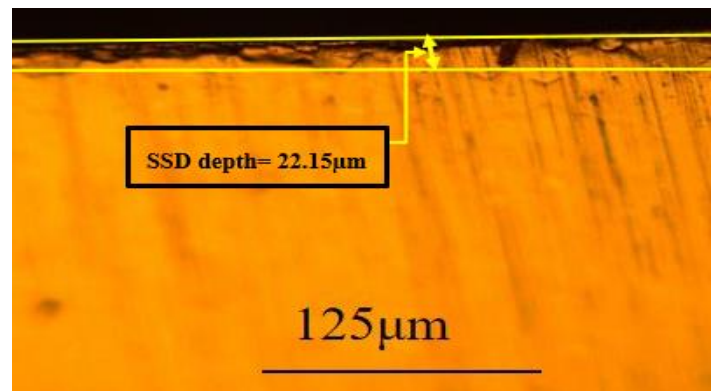
c. CG at Gd=20μm, Vs=6000rpm, Vw=20mm/min

d. CG at Gd=20μm, Vs=4000rpm, Vw=40mm/min

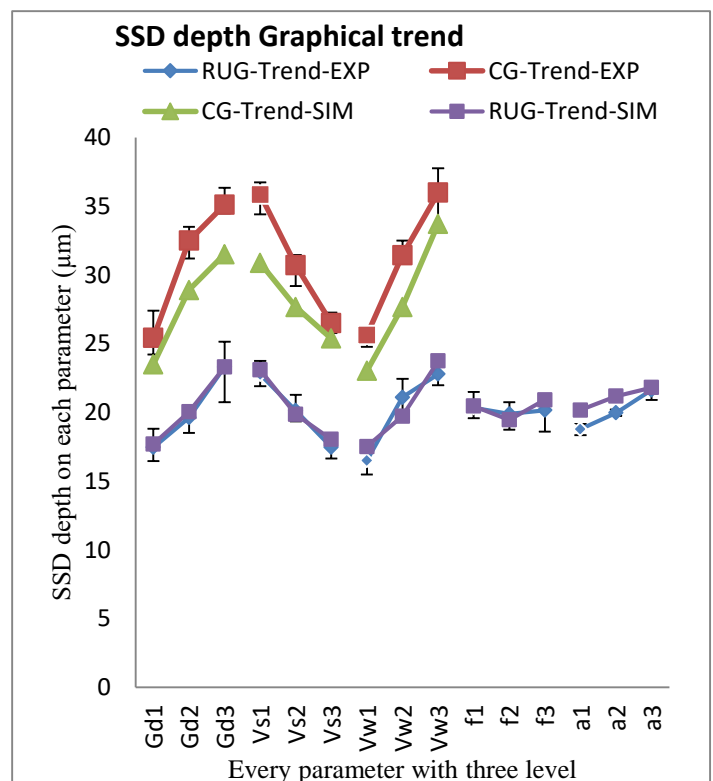Figure 9. Present SEM-SSD depth taken on different pa-rameters

Figure 10. Graphical trend on each parameter on SSD depth both simulation and experiment
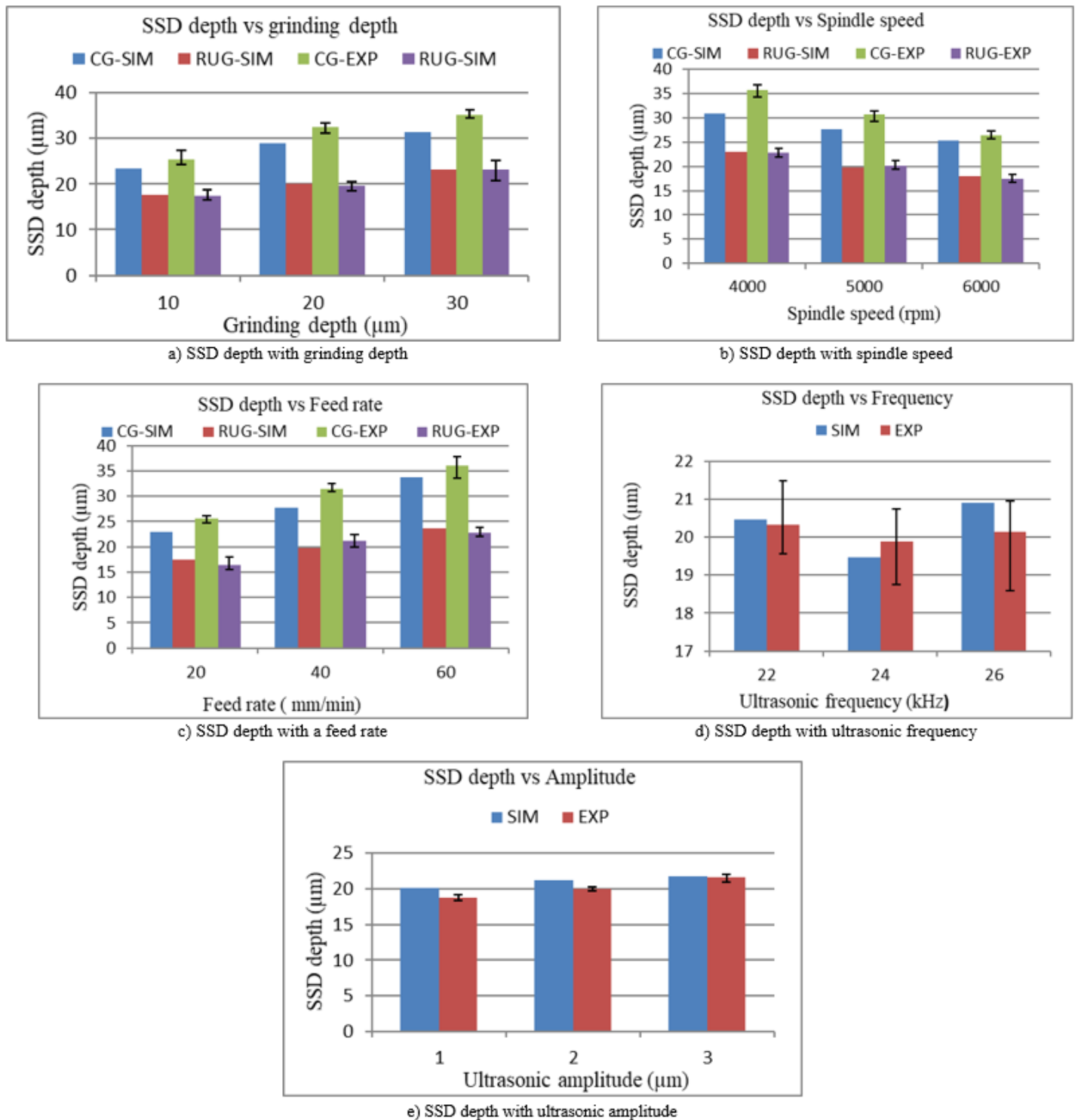
Figure 11. SSD Depth on both simulation and experi-ment grinding parameters

Hence, as mentioned above, the experiment results of grinding depth, feed rate, and spindle speed on subsur-face damage depth are well consistent with those exist-ing experimental works to Yao et al [26] and [27]. The results show that the subsurface damage depth values obtained under the rotary ultrasonic grinding methods are significantly smaller than those of ordinary grinding methods. Therefore, it can be inferred that under certain processing conditions,

the introduction of ultrasonic vibration effectively reduces the generation of sub-surface damage during the grinding process and obtains a better grinding surface. Therefore, this report believes that at the smaller grinding depth, feed rate, and higher spindle speed, the subsurface damage in grinding of tungsten alloy should be small, and the grinding surface integrity is better. It can be assumed that under certain processing conditions, the strength of ultrasonic vibra-tion

has an important impact on the subsurface dam-age, and the appropriate vibration intensity can more effectively reduce the generation of subsurface damage in W-Ni-Fe rotary ultrasonic grinding.

b. Effect of grinding parameters on subsurface damage

Refer to the statistical analysis done on each parameter with each level on the influence effect of grinding depth, spindle speed, feed rate, ultrasonic frequency, and am-plitude on subsurface damage through measuring SSD depth on both FEA simulations and experimental tests for both RUG and CG SSD depth is presented in figure 11.

The grinding depth plays an important role in SSD depth in brittle and ductile material grinding. The SSD depth grows in proportion to the grinding depth. When the grinding depth increases, the thickness of the mate-rial contacted by the abrasive particles on the outer side of the grinding wheel becomes larger, and the number of abrasive particles involved in the grinding increases, leading to an increase in the median crack damage as shown in figure 11(a). When the feed speed increases, the median crack depth becomes larger. With the in-crease of the feed speed, the actual grinding thickness of a single abrasive grain in the feed direction increases and leads to an increase in the SSD depth as shown in figure 11(c). Also, with the increase of the tool feed speed, the abrasive-material contact force would gener-ally increase, thus deteriorating the stress state in the interior material. The lateral cracks produced by the previous abrasives would provide the effects for the increased force imposed on the subsequent abrasives. on the other hand, the lateral grinding depth of each abrasive would decrease with the increased grinding spindle speed, reducing the mechanical loads exerted on the material which generates the reduction of SSD depth as illustrated in figure 11(b).

The superposing of an ultrasonic vibration would lead to the maximum grinding depth of each abrasive in-creased by the value of amplitude, this increasing of depth would expose both abrasive and workpiece to a high mechanical load which increases the depth of me-dian crack[28]. This is a clear reason for the increment of SSD depth for increasing the ultrasonic amplitude as shown in figure 11 (e).

Refer to the simulation and experimental tests results, the effects of grinding tool speed through spindle speed, grinding depth, feed rate, ultrasonic frequency, and ul-trasonic amplitude on subsurface damage are con-sistent on both simulation and experiment processes. Also, the introduction of ultrasonic grinding shows that the values of subsurface damage reduced compared to those conventional grinding. Therefore, the feed rate had the largest impact, followed by grinding depth, spindle speed, amplitude, and final ultrasonic frequency had little effect on SSD depth. Through subsurface damage orthogonal array simulation and experiment results, the comparison between RUG and CG is easily by correlating the test results obtained on analogous grinding conditions means the same parameter and level on grinding depth, spindle speed, and feed rate. This comparison showed that the RUG SSD depth re-duced about 27.79 % and 34.85 % of simulation and experimental tests respectively compared to CG SSD. And also presented a good agreement as to the average deviation on the SSD depth, which is 0.88% and 9.39% on RUG and CG respectively.

5. Conclusions

Based on the study of subsurface damage of tungsten alloy (W-Ni-Fe) done, shows a good agreement with FEA simulation and experiment tests conducted on both rotary ultrasonic grinding and conventional grind-ing machining processes. The complete work and relat-ed conclusions on simulation processes, experimental grinding tests, subsurface damage detection, and influ-ence effects of grinding parameters are summarized as follows:

a. On both FEA numerical simulations and experiment tests, the introduction of rotary ultrasonic vibration (RUG) can effectively save the labor energy required through the grinding force in the grinding process and also under the same grinding parameters on both simulation and experiment processes, results show that the in-troduction of rotary ultrasonic vibration can effectively reduce the subsurface damage.

b. Through different grinding parameters tests of W-Ni-Fe on both RUG and CG, show that the grinding depth, feed rate, spindle speed, and ultrasonic ampli-tude have more effect on subsurface damage but ultra-sonic frequency presents a little effect. Also, the feed rate is the most factor affecting the subsurface damage.

c. In this study, the W-Ni-Fe material is removed by brittle frac-ture.

In general, to reduce the grinding force and subsurface damage generated during the grinding process, not only reasonable process methods and processing parameters must be selected, but also tungsten alloy should be clar-ified as much as possible during the preparation of ma-terial. For the industry, this research has an immediate impact if the subsurface damage model is applied. By controlling the machining parameters, accepting the level of subsurface damage which can obtain according to the requirement of customers, and the number of defective parts should be reduced and increasing the productivity. The lower the grinding depth and feed rate, the higher the grinding spindle speed, and neither too small nor too big ultrasonic frequency and amplitude should reduce the subsurface damage depth.

Conflict of Interest Statement

The authors must declare that there is no conflict of interest in the study.

CRediT Author Statement

Emmanuel Karangwa: Conceptualization, Supervision, Writing-orig-inal draft, Writing-revised-paper
Pacifique Turabimana: Conceptualization, Writing-original draft, Validation, Writing-original draft, Writing-revised-paper

References

1. Y. Şahin, "Recent Progress in Processing of Tungsten Heavy Alloys," J. Powder Technol., vol. 2014, pp. 1–22, 2014.
2. L. Jieqiong, H. Jinguo, L. Mingming, G. Yan, and Z. Wenhui, "Development of nonresonant elliptical vibration cutting device based on a parallel piezoelectric actuator," AIP Adv., vol. 7, no. 3, 2017.
3. Z. J. Pei and P. M. Ferreira, "Experimental investigation of rotary ultrasonic face milling," Int. J. Mach. Tools Manuf., vol. 39, no. 8, pp. 1327–1344, 1999.
4. Z. J. Pei, P. M. Ferreira, S. G. Kapoor, and M. Haselkorn, "Rotary ultrasonic machining for face milling of ceramics," Int. J. Mach. Tools

Manuf., vol. 35, no. 7, pp. 1033–1046, 1995.

5. W. Cong, Z. Pei, and M. S. Engineering, "Handbook of Manufacturing Engineering and Technology," Handb. Manuf. Eng. Technol., no. Legge 1966, pp. 1–19, 2013.

6. J. F. Yin, Q. Bai, and B. Zhang, "Methods for detection of subsurface damage: A review," Chinese J. Mech. Eng. (English Ed., vol. 31, no. 3, 2018.

7. Y. Zhou, P. D. Funkenbusch, D. J. Quesnel, D. Golini, and A. Lindquist, "Effect of Etching and Imaging Mode on the Measurement of Subsurface Damage in Micro ground Optical Glasses," J. Am. Ceram. Soc., vol. 77, no. 12, pp. 3277–3280, 1994.

8. O. Al, H. Jeong, B. H. Koo, and C. G. Lee, "Mössbauer spectra of MnFe," vol. 4, pp. 1129–1132, 2010.

9. T. O. Mulhearn, "The deformation of metals by Vickers-type pyramidal indenters," J. Mech. Phys. Solids, vol. 7, no. 2, pp. 85–88, 1959.

10. C. F. Kronenberg and K. C. Jungling, "Subsurface damage identification in optically transparent materials using a non-destructive method," Appl. Opt., vol. 33, no. 19, p. 4248, 1994.

11. J. C. Lambropoulos, "w, 1.4," vol. 4680, no. 1987, 2000.

12. J. Wang, Y. Li, J. Han, Q. Xu, and Y. Guo, "Evaluating subsurface damage in optical glasses," Journal of the European Optical Society, vol. 6. 2011.

13. H. Xiao, Z. Chen, H. Wang, J. Wang, and N. Zhu, "Effect of grinding parameters on surface roughness and subsurface damage and their evaluation in fused silica," Opt. Express, vol. 26, no. 4, p. 4638, 2018.

14. C. Zhang, J. Zhang, and P. Feng, "Mathematical model for cutting force in rotary ultrasonic face milling of brittle materials," Int. J. Adv. Manuf. Technol., vol. 69, no. 1–4, pp. 161–170, 2013.

15. F. Lakhdari, D. Bouzid, N. Belkhir, and V. Herold, "Surface and subsurface damage in Zerodur® glass-ceramic during ultrasonic-assisted grinding," Int. J. Adv. Manuf. Technol., vol. 90, no. 5–8, pp. 1993–2000.

16. J. Wang, C. Zhang, P. Feng, and J. Zhang, "A model for prediction of subsurface damage in rotary ultrasonic face milling of optical K9 glass," Int. J. Adv. Manuf. Technol., vol. 83, no. 1–4, pp. 347–355, 2016.

17. Y. Liu, X. Wu, Q. Guo, C. Jiang, F. Song, and J. Li, "Experiments and numerical simulations of thermal shock crack patterns in thin circular ceramic specimens," Ceram. Int., vol. 41, no. 1, pp. 1107–1114,2015.

18. L. Wan, Z. Liu, Z. Deng, L. Li, and W. Liu, "Simulation and experimental research on subsurface damage of silicon nitride grinding," Ceram. Int., vol. 44, no. 7, pp. 8290–8296, 2018.

19. X. Jing, S. Maiti, and G. Subhash, "A new analytical model for estimation of scratch-induced damage in brittle solids," J. Am. Ceram. Soc., vol. 90, no. 3, pp. 885–892, 2007.

20. D. Mourtzis, M. Doukas, and D. Bernidaki, "Simulation in manufacturing: Review and challenges," Procedia CIRP, vol. 25, no. C, pp. 213–229, 2014.

21. V. Kushner and M. Storchak, "Modelling the material resistance to cutting," Int. J. Mech. Sci., vol. 126, no. March, pp. 44–54, 2017.

22. W. Grzesik, P. Niesłony, and P. Laskowski, "Determination of Material Constitutive Laws for Inconel 718 Superalloy Under Different Strain Rates and Working Temperatures," J. Mater. Eng. Perform., vol. 26, no. 12, pp. 5705–5714, 2017.

23. L. M. Bresciani, A. Manes, T. A. Romano, P. Iavarone, and M. Giglio, "Numerical modeling to reproduce fragmentation of a tungsten heavy alloy projectile impacting a ceramic tile: Adaptive solid mesh to the SPH technique and the cohesive law," Int. J. Impact Eng., vol. 87, pp. 3–13, 2016.

24. J. Li, F. Song, and C. Jiang, "Direct numerical simulations on crack formation in ceramic materials under thermal shock by using a non-local fracture model," J. Eur. Ceram. Soc., vol. 33, no. 13–14, pp. 2677–2687, 2013.

25. Y. Chen, "Prediction of Subsurface Damage During Machining Nickel-Based Superalloys," 2013.

26. D. Lv, Y. Huang, Y. Tang, and H. Wang, "Relationship between subsurface damage and surface roughness of glass BK7 in rotary ultrasonic machining and conventional grinding processes," Int. J. Adv. Manuf. Technol., vol. 67, no. 1–4, pp. 613–622, 2013.

27. W. Gu, Z. Yao, and H. Li, "Investigation of grinding modes in horizontal surface grinding of optical glass BK7," J. Mater. Process. Technol., vol. 211, no. 10, pp. 1629–1636, 2011.

28. D. Lv, H. Wang, W. Zhang, and Z. Yin, "Subsurface damage depth and distribution in rotary ultrasonic machining and conventional grinding of glass BK7," Int. J. Adv. Manuf. Technol., vol. 86, no. 9–12, pp. 2361–2371, 2016.